

Rheology Informed Mixture Engineering of Aggregates for Extrusion Additive Manufacturing.

S.U.M. Rabbi Hossain*†, Timothy Moore*†, Philip King*†

*Department of Mechanical Engineering, University of Maine, Orono, ME 04469

†Advanced Structures and Composites Center, University of Maine, Orono, ME 04469

Abstract

The ability to predict and control flow due to extrusion under load is one of the main barriers to closed loop control in additive manufacturing. Motivated by the premise that any material that can be granulated and bonded can be printed, this study investigates the rheological behavior of aggregate materials during extrusion. A ceramic media is tested with two different particle size distributions to examine how binder and particles interact while flowing under load. A custom-built extrusion rheometer is used to characterize material response through extrusion force, wall shear stress, and flow consistency. Flow characteristics of the ceramic media and the binder are evaluated to determine key material properties, such as shear thinning, in a continuous extrusion setup. The results demonstrate the impact of particle size on flow resistance and identify formulation-dependent parameters that govern extrudability. This work lays the foundation for rheology-informed design of printable materials, enabling adaptive extrusion platforms that can print a diverse range of materials.

1. Introduction

Extrusion-based additive manufacturing (AM) is a popular approach for fabricating complicated geometries from a wide range of materials. These include, but are not limited to, ceramics, polymers, and cementitious systems. The scalability and simplicity of this process make it suitable for sustainable construction and manufacturing that utilizes various mineral type materials. However, reliable extrusion requires balancing two contrasting properties of the material being printed: the material must flow easily under pressure (extrudability/flowability) and shape and structure retention after deposition (buildability). These properties can be quantified by studying the rheological properties such as yield stress, viscosity, thixotropy, and wall slip. [1][2][3][4][5].

Much of the existing research has focused on chemical admixtures and binder chemistry to tune these properties. Yet, an equally fundamental factor is particle size distribution (PSD), which defines how particles of different sizes are proportioned in a mix. PSD influences packing density, contact networks, and fluid demand. A broad PSD in concept improves packing efficiency by allowing smaller particles to fill voids between larger ones, reducing liquid demand and enhancing force chains. An excessive amount of fine particles contributes to a higher surface area and thus

elevated viscous forces due to higher interparticle interactions, sometimes causing clogging. PSD therefore plays a central role in determining extrusion stability

Despite its importance, PSD's effect is often studied alongside variations in binder content, chemistry, or liquid ratio, making it difficult to isolate. The extrusion of binder-lean, granular-rich ceramic pastes remains underexplored. To address this, the present study systematically investigates the influence of controlled PSD profiles on rheology and extrusion behavior using capillary rheometry, while keeping the binder system minimal and constant. The particles chosen also conform to a degree of sphericity to isolate the effects of anisotropic components. By decoupling PSD from chemical complexity, this work aims to provide a rheology-informed framework for designing sustainable, mineral-based extrusion AM processes.

2. Literature Review

Prior studies into mix components for ceramic extrusion have marked it as a strong factor for rheological thresholds and extrusion performance. Khecho et al. [6] demonstrated that fine, monomodal PSDs in highly loaded silica suspensions (>20-30 wt%) improved shear-thinning behavior, elastic moduli and filament quality. Ji et al. [7] established quantitative PSD-linked thresholds such as shear thinning index and yield modulus in binder-free ceramic pastes. Gündüz et al. [8] confirmed that finer kaolinite particles reduced wall slip and improved viscosity.

In alkali-activated systems, Kondepudi and Subramaniam [9] [10] showed that tailored PSDs reduced segregation and improved build up in fly ash-slag concretes by preventing segregation, improved phase cohesion and enhanced structural buildup. Sun et al. [11] and Ma et al. [12] reported that PSD effects are amplified when combined with binder control and rheology modifiers, enhancing cohesion and strength. Jayathilakage et al. [13] and Tripathy et al. [14] developed buildability models based on yield stress and failure curves, underscoring the role of thixotropic recovery. Chen et al. [15] and Shao et al. [16] introduced limestone fillers for specific PSDs and in-situ polymerization as strategies to shift rheological regimes toward better printability.

In order to develop a robust extrusion control system, there has to be a general model that mimics the behavior of the material design space. To generalize material design, Rau et al. [17] proposed a rheology “roadmap” of empirical thresholds for extrusion inks. Xu et al. [18] and Barjuei et al. [19] introduced AI-driven workflows that predict printability from rheological data, enabling automated construction. These frameworks expand PSD-focused insights into broader, system-level applications. Exploring a wider range of materials, Maierdan et al. [20] highlighted the role of PSD in alginate-stabilized earth concretes, while Soda et al. [21] confirmed that a tailored PSD and fine particle content improved strength and stability in excavated-soil systems. These works reinforce PSD as a key driver in sustainable, low-carbon extrusion.

Since the balance of forces during extrusion does not directly match with the action in traditional rheometers, the development of a capillary rheometer is essential. The data generated via this setup helps to make models which aid in the robust extrusion process. Janas [22] and Martin et al. [23] conducted pioneering studies on capillary extrusion of ceramic pastes, linking yield stress and particle migration to extrusion pressure. Cao et al. [24] proposed a rapid capillary-based method to predict extrusion pressure, while Yarahmadi et al. [25] and Faes et al. [26] directly tied PSD and yield recovery to filament geometry. Guerrini et al. [27] and Vitali et al. [28] validated capillary rheometry as a more representative tool for high-shear extrusion compared to other methods [5]. Ness et al. [29] explained flow regime transitions in dense suspensions using DEM, correlating friction and the shapes of particles to changes in extrusion pressure and die swell. This is consistent with Farris's classical prediction [30] that multimodal PSDs reduce viscosity.

In practice, rheology modifiers are often combined with PSD control to fine-tune performance. Kaci et al. [31] showed that polymer-bentonite interactions significantly affect shear-thinning response and wall stress in pastes. Chen et al. [32] reported that cellulose nanofibers (CNF)–clay networks improve cohesion and mitigate shrinkage while boosting recovery. Pignon et al. [33] provided foundational insight into clay suspensions, showing that thixotropy (shear breakdown followed by time-dependent recovery) is critical for layering stability. However, the combined role of PSD and modifiers in ceramic systems remains underexplored

In summary, while PSD is consistently shown to affect flow, packing, and printability across cements, soils, and ceramics, most studies confound it with binder chemistry or additive use. The isolated role of PSD in binder-lean, granular-rich ceramic pastes under extrusion-relevant conditions has not been systematically studied. This gap motivates the present work.

3. Methods

3.1 Materials

Two ceramic bead-binder mixtures were prepared using ceramic beads with fine (AFS GFN 85) and coarse (AFS GFN 40) grain sizes (Table 1). Both mixtures used the same binder formulation to ensure that particle size was the only varying factor. The specific ratio of the constituents were selected based on preliminary tests to ensure adequate flowability and cohesion. Each mixture was blended thoroughly using a high shear mixer to ensure uniformity before extrusion. The mixing is done in multiple stages as follows:

- Dry ingredients are mixed.
- CNF is added and mixed using a high shear mixer.
- Mixing is done at 135 Rpm in three stages, each stage lasts for 5 minutes.
- The material is manually folded between each step to ensure uniform distribution.
- Mixing is concluded when mix homogeneity is observed.

Component	Percentage
Ceramic Media	70.92%
Bentonite Clay	5.07%
CNF (2% wt. solid content)	23.61%
Carboxymethyl Cellulose (CMC)	0.41%

Table 1. Mix Composition

The ceramic media used in the experiments was Carbo Ceramics Accucast ID 80 (AFS GFN 85) and Carbo Ceramics Accucast ID40 (AFS GFN 40) (Figure 1) (Table 2). Carbo Ceramics Accucast ID 15 (AFS GFN 15) was also attempted to be used but the extrusion pressure it required exceeded the limits of the rheometer. This will be discussed further in the results and discussion section. The chemical composition of the ceramic media is Al_2O_3 (70-80%), SiO_2 (10-20%), TiO_2 (1-5%) Fe_2O_3 (5-10%) LOI (0.15%), Moisture (0.03%) pH 6.90 ADV@pH5 0.60, ADV@pH70.00. The bentonite clay and the CNF were used as binder for the paste and the CMC was employed to prevent phase separation at high loads experienced during extrusion.

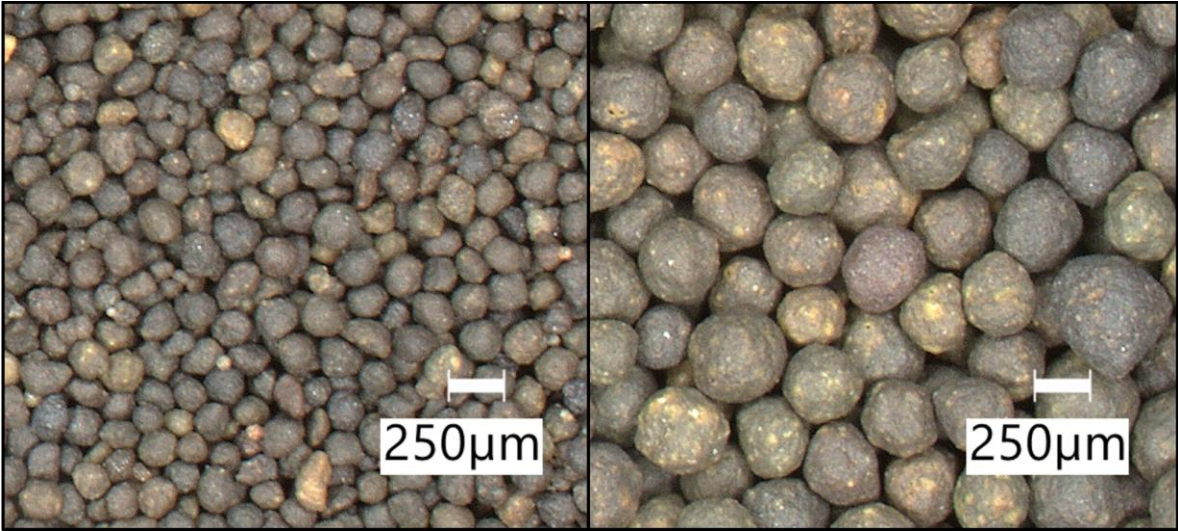


Figure 1. Comparison of ceramic particles at 20X magnification. (left) ID 80, (right) ID 40

Table 2. Particle Size Distribution for Ceramic Beads

Sieve No	16	18	20	30	40	50	70	100	140	200
Microns	1180	1000	850	600	425	300	212	150	106	75
ID15	1	22	85	14	-	-	-	-	-	-
ID40	-	-	-	-	19	72	8	1	-	-
ID80	-	-	-	-	-	-	1	51	43	5

3.2 Extrusion Setup

Extrusion tests were carried out using a custom-built extrusion rheometer (Figure 2). The system consisted of a cylindrical barrel with an internal diameter of 50.8 mm and a fixed orifice at the base with a diameter of 5 mm. A flat piston, driven by a universal testing machine (Instron 5882), was used to apply compressive force and extrude the material through the orifice. A 3D-printed TPU gasket was used to seal the piston and the tube, facilitating extrusion and eliminating material seepage between the piston and the wall. Throughout each test, force and piston displacement were recorded in real time, providing the necessary data to evaluate the material's flow resistance.

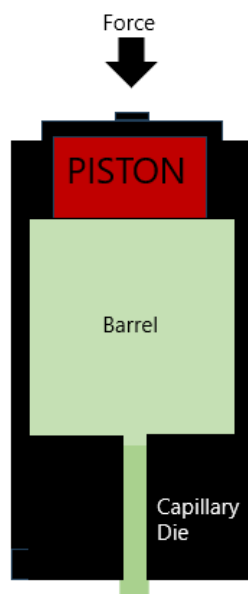


Figure 2. (Left) Diagram of Extrusion Rheometer, (Right) Custom Extrusion Rheometer

3.3 Testing Procedure

During testing, each ceramic mixture was tested at three controlled speeds (0.1 mm/s, 0.3 mm/s, and 0.5 mm/s), and a fixed piston displacement (50 mm) was applied. Such speeds were selected to represent a wide variety of flow conditions and to observe the behavior of the material under varying shear conditions. Instead of testing individual speeds one after another, the experiment was conducted with fixed, repeating speed sequences, repeated in three test cycles. Each cycle consisted of the three speeds applied in a different order (e.g., 0.1 → 0.3 → 0.5 in one run, followed by 0.3 → 0.5 → 0.1 in the next) (Table 3). The response to the different sequences of speeds could therefore be observed during testing.

Table 3. Experimental Design

	Test 1			Test 2			Test 3		
	Speed (mm/s)	Distance (mm)	Time (s)	Speed (mm/s)	Distance (mm)	Time (s)	Speed (mm/s)	Distance (mm)	Time (s)
Run 1	0.1	50	500	0.3	50	167	0.5	50	100
	0.3	50	167	0.5	50	100	0.1	50	500
	0.5	50	100	0.1	50	500	0.3	50	167
Run 2	0.3	50	167	0.5	50	100	0.1	50	500
	0.5	50	100	0.1	50	500	0.3	50	167
	0.1	50	500	0.3	50	167	0.5	50	100
Run 3	0.5	50	100	0.1	50	500	0.3	50	167
	0.1	50	500	0.3	50	167	0.5	50	100
	0.3	50	167	0.5	50	100	0.1	50	167

By repeating these sequences and varying the order, the tests captured not only the steady-state behavior of the mixtures but also any effects of cycling or prior flow history. This was also considered because of the assumption that more material in the tube may contribute to higher wall friction due to the increase in inter-grain contact surface. This has the potential to affect extrusion resistance and apparent viscosity. Another variable in the test is the Run number. This was introduced to test for rheological hysteresis and cyclic behavior, particularly for the presence of

CNF in the mixtures. The expectation was that if the material exhibited structural breakdown or thixotropic recovery, this would be reflected in the extrusion pressure needed across runs. Each testing segment at a specific speed lasted for a time calculated based on the 50 mm travel distance. This resulted in durations of 500 seconds for 0.1 mm/s, 167 seconds for 0.3 mm/s, and 100 seconds for 0.5 mm/s.

This methodology aimed to investigate factors beyond mere flow resistance at varying velocities. It facilitated the detection of order-dependent processes, including hysteresis, structural relaxation, and the slow deterioration of internal structure. If the material exhibited reduced resistance at 0.1 mm/s after a high-speed segment compared to its original state, this would indicate time-dependent or flow-induced alterations in the mixture. Moreover, reiterating the sequence diminished the impact of startup effects and enhanced the measurement reliability.

4. Results & Discussion

4.1 Overview of Experimental Design and Variables

The original design of the experiment included three ceramic media samples in increasing order of particle sizes. During testing, we were unable to extrude the mix with the largest particles, ID 15. The reasoning behind this is the orifice size used in our setup. The orifice being too small caused blocks near the nozzle, leading to a high buildup of pressure. This pressure exceeded the current limits of the machine. Consequently, the runs using the ID 15 ceramic beads were excluded from the presented results. This will be addressed in our future works with modified nozzle designs.

Extrusion behavior of two mixes (fine and coarse) was investigated at controlled plunger movement rates of 0.1 mm/s, 0.3 mm/s, and 0.5 mm/s. These speeds result in volumetric flow rates of 192.66 mm³/s, 576.81 mm³/s, and 963.33 mm³/s for 0.1 mm/s, 0.3 mm/s, and 0.5mm/s, respectively. The materials differ in particle gradient, as measured by sieve testing (Table 2); the coarser media contains larger particles (AFS GFN 40) which boost permeability, whereas the fine media has smaller particles (AFS GFN 80) which lower the permeability values. Extrusion force information was obtained for displacements ranging from 10 to 40 mm (Figure 3). This trimming was done to look at the steady state properties during extrusion. This data was used to calculate apparent viscosity and wall shear stress at the contraction region. These findings will provide the foundation for the rheology of future modifier applications and control mechanisms in AM (using particle-based pastes). It can also help in controlling the rheological reaction in various stages of the process.

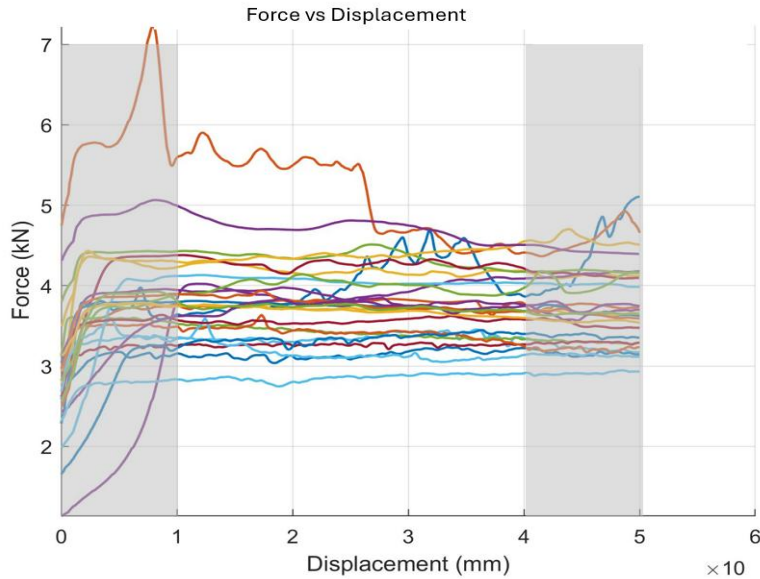


Figure 3. Trimmed data from 10 to 40mm.

4.2 Influence of Process Variables on Wall Shear Stress and Viscosity

An Analysis of Variance (ANOVA) was used to discern which variables impacted the rheological properties. The particle size and extrusion speed were found to significantly affect the wall shear stress and viscosity ($p < 0.0001$). Speed had the strongest effects on viscosity, but particle size also had significant impacts on the two properties, especially in wall shear stress. Regression coefficients show that at higher values of speed, viscosity steadily decreased, proving the shear-thinning property of the mixtures. Detailed Results of the ANOVA are provided in the appendix. The wall shear stresses were less affected by the speed with a positive trend due to inertial resistance during rapid extrusion.

The order and run number did not significantly affect wall shear stress or viscosity when the entire data set was considered ($p > 0.05$). However, when the data was examined by grouping fine ceramic particles as one data set and coarse ceramic particles as another independent dataset, run number became significant for the fine particle dataset for both viscosity ($p = 0.050$) and wall shear stress ($p = 0.020$) (Appendix). This suggests that wall shear stress and viscosity are sensitive to repeated loading of the finer particle systems. This is most likely because as the CNF passes through the die of the rheometer, the fibers shear, resulting in less flow resistance in subsequent cycles. This theory is further supported by examining if a difference exists between runs 2 and 3 for the fine particles. Figure 4 shows the CNF matrix and the ceramic beads before and after extrusion. In both images, we see the CNF and binder matrix encapsulating all the ceramic beads. On the right, we see an extruded bead. The bead has visible fibers oriented in the direction of the flow. This attests to the assumption that the fibers are subject to shear forces during extrusion. When an ANOVA is performed exclusively looking at runs 2 and 3 of the fine particles, the run number is found to have an insignificant effect on both wall shear stress and viscosity ($p > 0.05$).

This leads to the conclusion that once the CNF matrix passes through the die once, it breaks down to the point where the individual fibers are no longer significantly shearing. Another question that arises from this, though, is why the same phenomenon is not observed for the coarser particles. This is most likely due to the increased spacing between the particles for the coarser media, which allows the CNF fibers to flow more easily without being pinned against a particle.

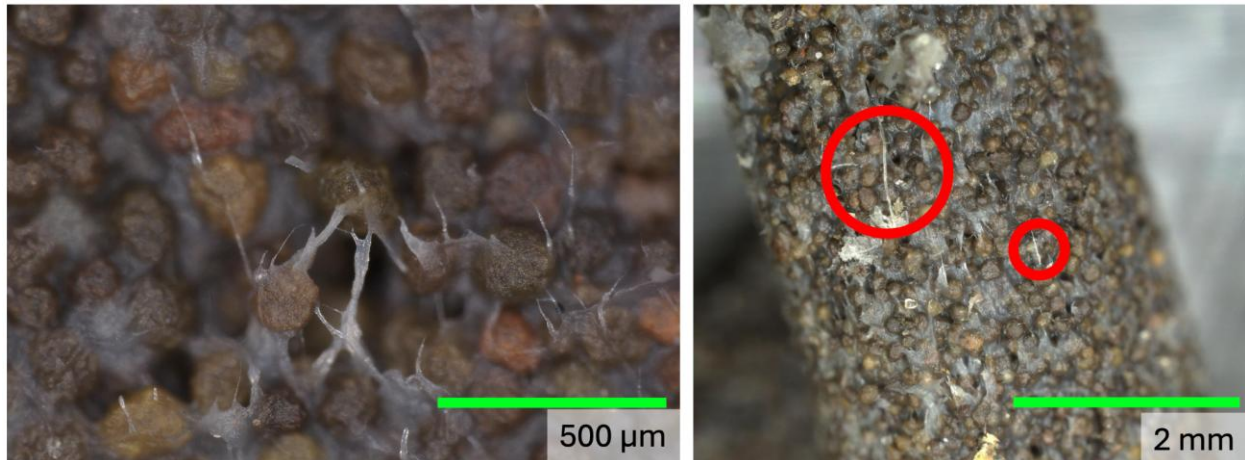


Figure 4. (left) Optical microscopy image of particle-binder-CNF mix at 200X magnification, (right) Optical microscopy image of particle-binder-CNF bead after extrusion at 20X magnification. Red circles indicate fibers aligned after extrusion.

4.3 Rheological Trends Across Particle Size and Speed

The ceramic beads are not unimodal in their size distribution, so we looked at the packing factor for both ID40 (Coarse) and ID80 (Fine) samples. The packing factor came out to 0.64 using both Andreassen and Dinger-Funk fits. These models do not consider the presence of any binder matrix in the mix but it does paint a picture of how the different sized particles fit together. The same value for both samples indicate that the particles occupy the same volume fraction in both distributions, which indicates the same amount of binder volume fraction. However, the rheological and the mechanical properties might still differ due to several factors like surface area, contact surface, permeability, and cohesion.

The apparent viscosity reached a maximum value at 0.1 mm/s in both materials, and the values decreased as the plunger speed increased. The finer material tended to produce higher viscosities and wall shear stress compared to that of the coarser counterpart. This behavior is attributed to the increased surface area and diminished permeability of the finer media with smaller grains, which increases interparticle friction and thus increases flow resistance (Figure 5). Also associated with this trend were the wall shear stress levels; the fine media consistently exhibited higher wall shear stress than the coarse media at the same extrusion speeds (Figure 6).

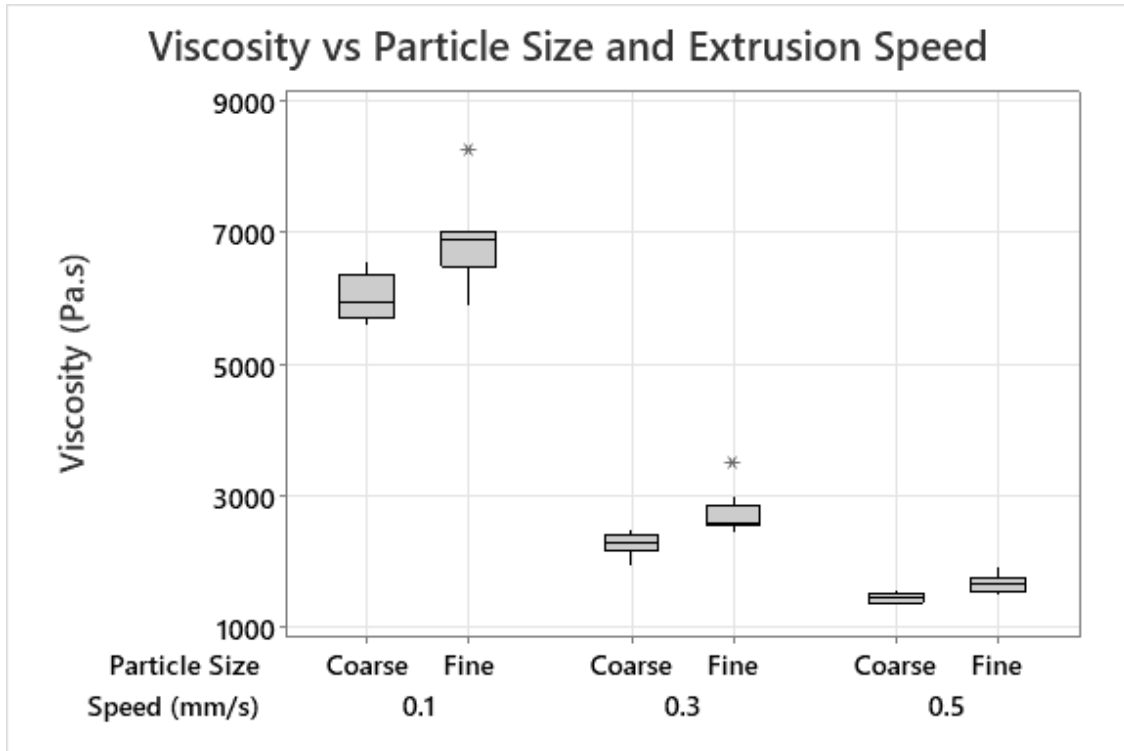


Figure 5. Box plot showing viscosity vs particle size at different extrusion speeds

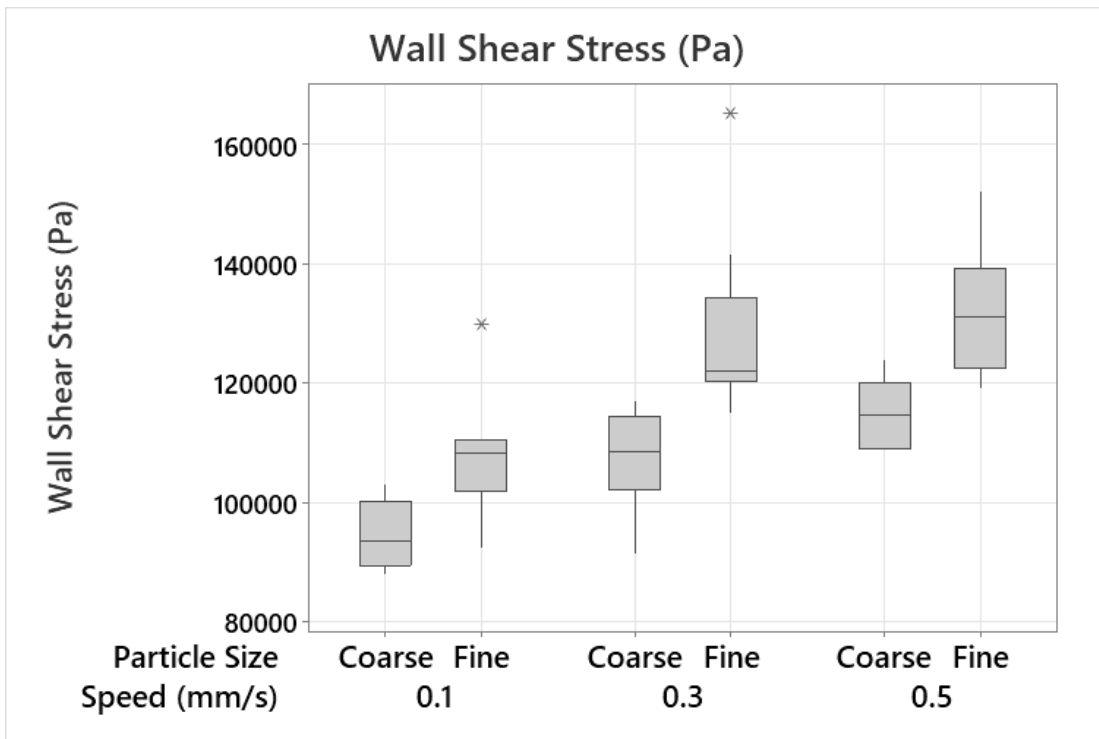


Figure 6. Box plot showing wall shear stress vs particle size at different extrusion speeds

The viscosity and wall shear stress values were also examined across three different speeds to uncover any trends or patterns. The viscosity values decrease with increasing speeds while the wall shear stress values increase with increasing speeds (Figure 5). The speed is analogous to shear rate, so the viscosity trend corresponds to a shear-thinning behavior. At higher speeds, the standard deviations of the viscosity shrink, implying the process is reaching a steady state. The increasing trend in the wall shear stress indicates higher force and energy expended to make the material flow at a higher speed. This indicates that the material resists flow by either becoming more densely packed or the friction between the grains and the matrix increases with higher extrusion speeds. This area needs more exploration using rheological modifiers and a wider range of speeds.

Looking at the viscosity and the wall shear stress across the two different particle size distributions, different responses are seen yet again (Figure 5 and 6). The viscosity values are similar, except for the finer material having a higher peak and wider interquartile range. Since the packing factor for both samples is identical, the similarity in the values of viscosity can be attributed to the samples having the same binder volume ratios. The increase in the peak and the range can be explained by the higher surface area of the finer sample which leads to more interparticle interactions. The wall shear stress has higher values for the finer sample. Considering the identical packing factor for both samples, this increase can be attributed to increased surface area leading to higher contact surface among binder and beads, increased wall friction, decreased permeability and increased cohesion among particles.

4.4 Comparative Flow Dynamics: Fine vs Coarse

The rheological responses in the coarse and the fine media were different, although they had the same binder formulations. The finer media showed more resistance to flow because it has an increased surface area, which leads to increased contact between the binder and beads and thus requires more energy to maintain the corresponding volumetric flow rate. This is supported by the reduced permeability of the fine media compared to the coarse media. The fine media has a permeability number of 52, as compared to 285 for coarse media. Thus, its internal flow paths are more compact, resulting in high cohesion leading to high back pressure during extrusion. To initiate and maintain flow, the force required in the fine media was not only higher on average but was increased in variability and thus less predictable unless there are compensatory efforts to take it under some type of control. This increased variability was most likely due to the increased interactions between the particles.

On the contrary, coarse sand exhibited greater rheological consistency. Its coarser grains led to a more stable onset of flow, but at the possible expense of weaker interlayer bonding in printed parts. The lower wall shear stress and viscosity figures show it is best to use a coarser grain where extrusion ease is considered of more importance than geometric accuracy or finish.

5. Conclusion and Future Work

The key findings of this study lead to several important conclusions. We were able to isolate the impact of PSD on the extrusion process. Finer particles, due to the high surface area and higher interparticle interaction, exhibit a higher wall shear stress under extrusion. This insight will aid in engineering future mixes and extrusion systems for said mixes. We also found that this, does not alter the shear thinning behavior of the sample in general, meaning that rheological modifiers need to be investigated that can lower the stress values in the finer media by improving the binder-bead and inter-bead interactions. The high particle loading of the mix (~70 % solid mass) leads to the high energy requirement for extrusion. The rheometer used in this study will be used to further explore the material design space and the effects of new modifiers.

The study was limited to steady-state extrusion at three discrete speeds and a fixed displacement range. The influence of temperature, moisture content, and long-term flow degradation was not considered. The goal was to set a baseline for further exploration in the material design space. Future work will incorporate extended displacement tests and in-nozzle pressure monitoring. We also plan to use a gradient in the applied force to isolate the effects of inertia while switching between speeds and its effects on the corresponding flow rate. The nature of flow and the reaction of the material to extrusion force will be analyzed with pressure measurements from the extrusion site with the help of specialized equipment. The obtained data from the extended testing will be used to generate predictive models, which will culminate into a robust feedback control system for the extrusion of particle-rich granular materials.

Acknowledgements

This work is funded by the United States Army Engineering Research and Development Center (ERDC).

References

- [1] B. Khoshnevis, “Automated construction by contour crafting—related robotics and information technologies,” *Automation in Construction*, vol. 13, no. 1, pp. 5–19, Jan. 2004, doi: 10.1016/j.autcon.2003.08.012.
- [2] T. Wangler, N. Roussel, F. P. Bos, T. A. M. Salet, and R. J. Flatt, “Digital Concrete: A Review,” *Cement and Concrete Research*, vol. 123, p. 105780, Sep. 2019, doi: 10.1016/j.cemconres.2019.105780.
- [3] S. Nair, S. Panda, A. Tripathi, and N. Neithalath, “Relating print velocity and extrusion characteristics of 3D-printable cementitious binders: Implications towards testing methods,” *Additive Manufacturing*, vol. 46, p. 102127, Oct. 2021, doi: 10.1016/j.addma.2021.102127.
- [4] J. Bonilla-Cruz, M. A. Avila-López, F. E. L. Rodríguez, A. Aguilar-Elguezabal, and Tania. E. Lara-Ceniceros, “3D printable ceramic pastes design: Correlating rheology & printability,” *Journal of the European Ceramic Society*, vol. 42, no. 13, pp. 6033–6039, Oct. 2022, doi: 10.1016/j.jeurceramsoc.2022.06.029.

- [5] A. U. Khan, B. J. Briscoe, and P. F. Luckham, "Evaluation of slip in capillary extrusion of ceramic pastes," *Journal of the European Ceramic Society*, vol. 21, no. 4, pp. 483–491, Apr. 2001, doi: 10.1016/s0955-2219(00)00213-2.
- [6] A. Khecho, S. A. Ghaffari, and B. Eftekhari Yekta, "The influence of particle size distribution on rheological properties of fused silica pastes for direct ink writing," *International Journal of Applied Ceramic Technology*, vol. 19, no. 5, pp. 2472–2479, 2022, doi: 10.1111/ijac.14109.
- [7] H. Ji *et al.*, "A novel experimental approach to quantitatively evaluate the printability of inks in 3D printing using two criteria," *Additive Manufacturing*, vol. 55, p. 102846, Jul. 2022, doi: 10.1016/j.addma.2022.102846.
- [8] Z. Gunduz, M. Alkan, and M. Dogan, "FLOW BEHAVIOUR AND RHEOLOGICAL ASSESMENT OF KAOLINITE/PDMS PASTES VIA CAPILLARY RHEOMETER," *Fresenius Environmental Bulletin*, vol. 25, no. 10.
- [9] K. Kondepudi, K. V. L. Subramaniam, B. Nematollahi, S. H. Bong, and J. Sanjayan, "Study of particle packing and paste rheology in alkali activated mixtures to meet the rheology demands of 3D Concrete Printing," *Cement and Concrete Composites*, vol. 131, p. 104581, Aug. 2022, doi: 10.1016/j.cemconcomp.2022.104581.
- [10] R. Alfani, "Rheological test methods for the characterization of extrudable cement-based materials - A review," *Mater. Struct.*, vol. 38, no. 276, pp. 239–247, Jan. 2005, doi: 10.1617/14191.
- [11] S. Vitali and L. Giorgini, "Overview of the rheological behaviour of ceramic slurries," *FME Transactions*, vol. 47, no. 1, pp. 42–47, 2019, doi: 10.5937/fmet1901042v.
- [12] S. Ma *et al.*, "Unveiling the critical role of rheology modifiers in additive manufacturing of geopolymers and their mechanical properties," *Additive Manufacturing*, vol. 78, p. 103826, Sep. 2023, doi: 10.1016/j.addma.2023.103826.
- [13] R. Jayathilakage, P. Rajeev, and J. G. Sanjayan, "Yield stress criteria to assess the buildability of 3D concrete printing," *Construction and Building Materials*, vol. 240, p. 117989, Apr. 2020, doi: 10.1016/j.conbuildmat.2019.117989.
- [14] A. Tripathi, S. A. O. Nair, and N. Neithalath, "A comprehensive analysis of buildability of 3D-printed concrete and the use of bi-linear stress-strain criterion-based failure curves towards their prediction," *Cement and Concrete Composites*, vol. 128, p. 104424, Apr. 2022, doi: 10.1016/j.cemconcomp.2022.104424.
- [15] Y. Chen, Z. Li, S. Chaves Figueiredo, O. Çopuroğlu, F. Veer, and E. Schlangen, "Limestone and Calcined Clay-Based Sustainable Cementitious Materials for 3D Concrete Printing: A Fundamental Study of Extrudability and Early-Age Strength Development," *Applied Sciences*, vol. 9, no. 9, p. 1809, Jan. 2019, doi: 10.3390/app9091809.
- [16] L. Shao *et al.*, "A new strategy to enhance 3D printability of cement-based materials: In-situ polymerization," *Additive Manufacturing*, vol. 89, p. 104299, Jun. 2024, doi: 10.1016/j.addma.2024.104299.
- [17] D. A. Rau, M. J. Bortner, and C. B. Williams, "A rheology roadmap for evaluating the printability of material extrusion inks," *Additive Manufacturing*, vol. 75, p. 103745, Aug. 2023, doi: 10.1016/j.addma.2023.103745.
- [18] W. Xu *et al.*, "Toward automated construction: The design-to-printing workflow for a robotic in-situ 3D printed house," *Case Studies in Construction Materials*, vol. 17, p. e01442, 2022, doi: <https://doi.org/10.1016/j.cscm.2022.e01442>.

- [19] E. S. Barjuei, A. Capitanelli, R. Bertolucci, E. Courteille, F. Mastrogiovanni, and M. Maratea, “Digital workflow for printability checking and prefabrication in robotic construction 3D printing based on Artificial Intelligence planning,” *Engineering Applications of Artificial Intelligence*, vol. 133, p. 108254, Jul. 2024, doi: 10.1016/j.engappai.2024.108254.
- [20] Y. Maierdan *et al.*, “Rheology and 3D printing of alginate bio-stabilized earth concrete,” *Cement and Concrete Research*, vol. 175, p. 107380, 2024, doi: <https://doi.org/10.1016/j.cemconres.2023.107380>.
- [21] P. R. K. Soda, A. Dwivedi, S. C M, and S. Gupta, “Development of 3D printable stabilized earth-based construction materials using excavated soil: Evaluation of fresh and hardened properties,” *Science of The Total Environment*, vol. 924, p. 171654, May 2024, doi: 10.1016/j.scitotenv.2024.171654.
- [21] V. F. Janas, C. J. Malarkey, D. R. Treacy, and M. E. Zak, “Characterization of Ceramic Batch Via Capillary Rheometry,” *MRS Online Proceedings Library (OPL)*, vol. 289, p. 123, Jan. 1992, doi: 10.1557/PROC-289-123.
- [22] A. J. Martin, W. Li, J. Watts, G. E. Hilmas, M. C. Leu, and T. Huang, “Particle migration in large cross-section ceramic on-demand extrusion components,” *Journal of the European Ceramic Society*, vol. 43, no. 3, pp. 1087–1097, Mar. 2023, doi: 10.1016/j.jeurceramsoc.2022.10.059.
- [23] K. Cao, Y. Liu, C. Tucker, M. Baumann, G. Grit, and S. Lakso, “High-Throughput Method to Predict Extrusion Pressure of Ceramic Pastes,” *ACS Comb. Sci.*, vol. 16, no. 4, pp. 198–204, Apr. 2014, doi: 10.1021/co400031s.
- [25] M. Yarahmadi, P. Barcelona, G. Fargas, E. Xuriguera, and J. J. Roa, “Optimization of the ceramic ink used in Direct Ink Writing through rheological properties characterization of zirconia-based ceramic materials,” *Ceramics International*, vol. 48, no. 4, pp. 4775–4781, Feb. 2022, doi: 10.1016/j.ceramint.2021.11.013.
- [26] M. Faes, H. Valkenaers, F. Vogeler, J. Vleugels, and E. Ferraris, “Extrusion-based 3D Printing of Ceramic Components,” *Procedia CIRP*, vol. 28, pp. 76–81, 2015, doi: 10.1016/j.procir.2015.04.028.
- [27] K. Kondepudi and K. V. L. Subramaniam, “Formulation of alkali-activated fly ash-slag binders for 3D concrete printing,” *Cement and Concrete Composites*, vol. 119, p. 103983, May 2021, doi: 10.1016/j.cemconcomp.2021.103983.
- [28] C. Sun, J. Xiang, M. Xu, Y. He, Z. Tong, and X. Cui, “3D extrusion free forming of geopolymer composites: Materials modification and processing optimization,” *Journal of Cleaner Production*, vol. 258, p. 120986, Jun. 2020, doi: 10.1016/j.jclepro.2020.120986.
- [29] C. Ness and J. Sun, “Flow regime transitions in dense non-Brownian suspensions: Rheology, microstructural characterization, and constitutive modeling,” *Phys. Rev. E*, vol. 91, no. 1, Jan. 2015, doi: 10.1103/physreve.91.012201.
- [30] R. J. Farris, “Prediction of the Viscosity of Multimodal Suspensions from Unimodal Viscosity Data,” *Transactions of The Society of Rheology*, vol. 12, no. 2, pp. 281–301, Jul. 1968, doi: 10.1122/1.549109.
- [31] A. Kaci, M. Chaouche, and P.-A. Andréani, “Influence of bentonite clay on the rheological behaviour of fresh mortars,” *Cement and Concrete Research*, vol. 41, no. 4, pp. 373–379, Apr. 2011, doi: 10.1016/j.cemconres.2011.01.002.

- [32] Y. Chen *et al.*, “Rheology control and shrinkage mitigation of 3D printed geopolymer concrete using nanocellulose and magnesium oxide,” *Construction and Building Materials*, vol. 429, p. 136421, May 2024, doi: 10.1016/j.conbuildmat.2024.136421.
- [33] F. Pignon, A. Magnin, and J.-M. Piau, “Thixotropic behavior of clay dispersions: Combinations of scattering and rheometric techniques,” *Journal of Rheology*, vol. 42, no. 6, pp. 1349–1373, Nov. 1998, doi: 10.1122/1.550964.

Appendix

ANOVA Yield Stress (All factors)

Method

Factor coding (-1, 0, +1)

Factor Information

Factor	Type	Levels	Values
Speed (mm/s)	Fixed	3	0.1, 0.3, 0.5
Run Number	Fixed	3	1, 2, 3
Order	Fixed	3	1, 2, 3
Particle Size	Fixed	2	ID 40, ID 80

Analysis of Variance

Source	DF	Adj SS	Adj MS	F-Value	P-Value
Speed (mm/s)	2	4872509441	2436254720	26.82	0.000
Run Number	2	297892825	148946412	1.64	0.205
Order	2	403884657	201942329	2.22	0.120
Particle Size	1	3919569388	3919569388	43.16	0.000
Error	46	4177833113	90822459		
Total	53	13671689423			

Model Summary

S	R-sq	R-sq(adj)	R-sq(pred)
9530.08	69.44%	64.79%	57.89%

Coefficients

Term	Coef	SE Coef	T-Value	P-Value	VIF
Constant	114295	1297	88.13	0.000	
Speed (mm/s)					
0.1	-13003	1834	-7.09	0.000	1.33
0.3	3578	1834	1.95	0.057	1.33
Run Number					
1	3239	1834	1.77	0.084	1.33
2	-983	1834	-0.54	0.594	1.33
Order					
1	2695	1834	1.47	0.149	1.33
2	1055	1834	0.58	0.568	1.33
Particle Size					
ID 40	-8520	1297	-6.57	0.000	1.00

Regression Equation

Yield Stress (Pa) = 114295 - 13003 Speed (mm/s)_0.1 + 3578 Speed (mm/s)_0.3 + 9425 Speed (mm/s)_0.5 + 3239 Run Number_1 - 983 Run Number_2 - 2256 Run Number_3 + 2695 Order_1 + 1055 Order_2 - 3750 Order_3 - 8520 Particle Size_ID 40 + 8520 Particle Size_ID 80

Fits and Diagnostics for Unusual Observations

Yield Stress					
Obs	(Pa)	Fit	Resid	Std Resid	
2	91530	113648	-22118	-2.51	R
29	165474	130687	34787	3.95	R

ANOVA Viscosity (All factors)

Method

Factor coding (-1, 0, +1)

Factor Information

Factor	Type	Levels	Values
Speed (mm/s)	Fixed	3	0.1, 0.3, 0.5
Run Number	Fixed	3	1, 2, 3
Order	Fixed	3	1, 2, 3
Particle Size	Fixed	2	ID 40, ID 80

Analysis of Variance

Source	DF	Adj SS	Adj MS	F-Value	P-Value
Speed (mm/s)	2	241251655	120625827	1023.44	0.000
Run Number	2	388151	194076	1.65	0.204
Order	2	681999	340999	2.89	0.066
Particle Size	1	3297753	3297753	27.98	0.000
Error	46	5421721	117864		
Total	53	251041278			

Model Summary

S	R-sq	R-sq(adj)	R-sq(pred)
343.313	97.84%	97.51%	97.02%

Coefficients

Term	Coef	SE Coef	T-Value	P-Value	VIF
Constant	3510.3	46.7	75.14	0.000	
Speed (mm/s)					
0.1	2940.3	66.1	44.50	0.000	1.33
0.3	-1004.0	66.1	-15.20	0.000	1.33
Run Number					
1	116.1	66.1	1.76	0.086	1.33
2	-32.0	66.1	-0.48	0.630	1.33
Order					
1	134.7	66.1	2.04	0.047	1.33
2	5.6	66.1	0.09	0.933	1.33
Particle Size					
ID 40	-247.1	46.7	-5.29	0.000	1.00

Regression Equation

Viscosity (Pa.s) = 3510.3 + 2940.3 Speed (mm/s)_0.1 - 1004.0 Speed (mm/s)_0.3 - 1936.3 Speed (mm/s)_0.5 + 116.1 Run Number_1 - 32.0 Run Number_2 - 84.1 Run Number_3 + 134.7 Order_1 + 5.6 Order_2 - 140.4 Order_3 - 247.1 Particle Size_ID 40 + 247.1 Particle Size_ID 80

Fits and Diagnostics for Unusual Observations

Viscosity					
Obs	(Pa.s)	Fit	Resid	Std Resid	
28	8283	6949	1334	4.21	R
29	3520	2875	645	2.03	R

ANOVA Yield Stress (Only ID 40)

Method

Factor coding (-1, 0, +1)

Factor Information

Factor	Type	Levels	Values
Order	Fixed	3	1, 2, 3
Run Number	Fixed	3	1, 2, 3
Speed (mm/s)	Fixed	3	0.1, 0.3, 0.5

Analysis of Variance

Source	DF	Adj SS	Adj MS	F-Value	P-Value
Order	2	49460293	24730147	0.54	0.592
Run Number	2	57814713	28907357	0.63	0.543
Speed (mm/s)	2	1875392332	937696166	20.42	0.000
Error	20	918574789	45928739		
Total	26	2901242127			

Model Summary

S	R-sq	R-sq(adj)	R-sq(pred)
6777.07	68.34%	58.84%	42.30%

Coefficients

Term	Coef	SE Coef	T-Value	P-Value	VIF
Constant	105775	1304	81.10	0.000	
Order					
1	1883	1844	1.02	0.319	1.33
2	-644	1844	-0.35	0.731	1.33
Run Number					
1	-1965	1844	-1.07	0.299	1.33
2	421	1844	0.23	0.822	1.33
Speed (mm/s)					
0.1	-10893	1844	-5.91	0.000	1.33
0.3	1549	1844	0.84	0.411	1.33

Regression Equation

$$\begin{aligned} \text{Yield Stress (Pa)} = & 105775 + 1883 \text{ Order}_1 - 644 \text{ Order}_2 - 1239 \text{ Order}_3 \\ & - 1965 \text{ Run Number}_1 \\ & + 421 \text{ Run Number}_2 + 1544 \text{ Run Number}_3 - 10893 \text{ Speed (mm/s)}_{0.1} \\ & + 1549 \text{ Speed (mm/s)}_{0.3} + 9344 \text{ Speed (mm/s)}_{0.5} \end{aligned}$$

Fits and Diagnostics for Unusual Observations

Obs	Yield Stress (Pa)	Fit	Resid	Std Resid
2	91530	104715	-13185	-2.26 R

ANOVA Viscosity (Only ID 40)

Method

Factor coding (-1, 0, +1)

Factor Information

Factor	Type	Levels	Values
Order	Fixed	3	1, 2, 3
Run Number	Fixed	3	1, 2, 3
Speed (mm/s)	Fixed	3	0.1, 0.3, 0.5

Analysis of Variance

Source	DF	Adj SS	Adj MS	F-Value	P-Value
Order	2	162491	81245	1.47	0.254
Run Number	2	17898	8949	0.16	0.852
Speed (mm/s)	2	107259357	53629678	969.98	0.000
Error	20	1105795	55290		
Total	26	108545540			

Model Summary

S	R-sq	R-sq(adj)	R-sq(pred)
235.138	98.98%	98.68%	98.14%

Coefficients

Term	Coef	SE Coef	T-Value	P-Value	VIF
Constant	3263.2	45.3	72.11	0.000	
Order					
1	74.6	64.0	1.17	0.257	1.33
2	32.3	64.0	0.51	0.619	1.33
Run Number					
1	-21.6	64.0	-0.34	0.739	1.33
2	-14.5	64.0	-0.23	0.823	1.33
Speed (mm/s)					
0.1	2779.0	64.0	43.42	0.000	1.33
0.3	-981.2	64.0	-15.33	0.000	1.33

Regression Equation

Viscosity (Pa.s) = 3263.2 + 74.6 Order_1 + 32.3 Order_2 - 107.0 Order_3 - 21.6 Run Number_1 - 14.5 Run Number_2 + 36.2 Run Number_3 + 2779.0 Speed (mm/s)_0.1 - 981.2 Speed (mm/s)_0.3 - 1797.8 Speed (mm/s)_0.5

Fits and Diagnostics for Unusual Observations

Viscosity					
Obs	(Pa.s)	Fit	Resid	Std Resid	
20	6570	6053	517	2.56	R

ANOVA Yield Stress (Only ID 80)

Method

Factor coding (-1, 0, +1)

Factor Information

Factor	Type	Levels	Values
Order	Fixed	3	1, 2, 3
Run Number	Fixed	3	1, 2, 3
Speed (mm/s)	Fixed	3	0.1, 0.3, 0.5

Analysis of Variance

Source	DF	Adj SS	Adj MS	F-Value	P-Value
Order	2	531741202	265870601	2.48	0.109
Run Number	2	1023098601	511549300	4.77	0.020
Speed (mm/s)	2	3151454171	1575727086	14.69	0.000
Error	20	2144583934	107229197		
Total	26	6850877908			

Model Summary

S	R-sq	R-sq(adj)	R-sq(pred)
10355.2	68.70%	59.31%	42.95%

Coefficients

Term	Coef	SE Coef	T-Value	P-Value	VIF
Constant	122815	1993	61.63	0.000	
Order					
1	3507	2818	1.24	0.228	1.33
2	2754	2818	0.98	0.340	1.33
Run Number					
1	8444	2818	3.00	0.007	1.33
2	-2388	2818	-0.85	0.407	1.33
Speed (mm/s)					
0.1	-15112	2818	-5.36	0.000	1.33
0.3	5607	2818	1.99	0.060	1.33

Regression Equation

Yield Stress (Pa) = 122815 + 3507 Order_1 + 2754 Order_2 - 6261 Order_3 + 8444 Run Number_1

- 2388 Run Number_2 - 6056 Run Number_3 - 15112 Speed (mm/s)_0.1
 + 5607 Speed (mm/s)_0.3 + 9505 Speed (mm/s)_0.5

Fits and Diagnostics for Unusual Observations

Yield Stress					
Obs	(Pa)	Fit	Resid	Std Resid	
2	165474	139620	25854	2.90	R

ANOVA Viscosity (Only ID 80)

Method

Factor coding (-1, 0, +1)

Factor Information

Factor	Type	Levels	Values
Order	Fixed	3	1, 2, 3
Run Number	Fixed	3	1, 2, 3
Speed (mm/s)	Fixed	3	0.1, 0.3, 0.5

Analysis of Variance

Source	DF	Adj SS	Adj MS	F-Value	P-Value
Order	2	617513	308757	2.22	0.135
Run Number	2	977388	488694	3.51	0.050
Speed (mm/s)	2	134815389	67407694	483.61	0.000
Error	20	2787695	139385		
Total	26	139197985			

Model Summary

S	R-sq	R-sq(adj)	R-sq(pred)
373.343	98.00%	97.40%	96.35%

Coefficients

Term	Coef	SE Coef	T-Value	P-Value	VIF
Constant	3757.4	71.8	52.30	0.000	
Order					
1	195	102	1.92	0.070	1.33
2	-21	102	-0.21	0.838	1.33
Run Number					
1	254	102	2.50	0.021	1.33
2	-49	102	-0.49	0.632	1.33
Speed (mm/s)					
0.1	3102	102	30.52	0.000	1.33
0.3	-1027	102	-10.11	0.000	1.33

Regression Equation

Viscosity (Pa.s) = 3757.4 + 195 Order_1 - 21 Order_2 - 174 Order_3 + 254 Run Number_1
 - 49 Run Number_2 - 204 Run Number_3 + 3102 Speed (mm/s)_0.1
 - 1027 Speed (mm/s)_0.3 - 2075 Speed (mm/s)_0.5

Fits and Diagnostics for Unusual Observations

Viscosity					
Obs	(Pa.s)	Fit	Resid	Std Resid	
1	8283	7308	975	3.04	R